

Duffing Oscillator Vibration Control via Suspended Pendulum

Wedad Ali El-Ganaini

Department of Physics and Engineering Mathematics, Faculty of Electronic Engineering, Menoufia University, Menouf, 32952, Egypt.

Received: 3 Oct. 2017, Revised: 2 Nov. 2017, Accepted: 18 Nov. 2017

Published online: 1 Jan. 2018

Abstract: This paper investigates the vibration control of a harmonically excited Duffing oscillator via a simple pendulum. The amplitude-phase modulating equations governing the system dynamics are extracted utilizing perturbation methods. Bifurcation analyses are conducted and the Lyapunov direct method is applied to study the system stability. The uncontrolled system exhibits a variety of nonlinear phenomena such as jump phenomenon, saddle-node, and transcritical bifurcations. The analysis showed that the oscillator vibrational energy could be transferred to the pendulum parametrically when the pendulum natural frequency is equal to one-half the oscillator natural frequency. Numerical validation for the obtained analytical results was performed, which is in excellent agreement with the analytical ones. By the end of this work, a comparison with published work is included.

Keywords: autoparametric, saturation phenomena, resonance, saddle-node bifurcation, transcritical bifurcation.

1 Introduction

Vibrations are initiated when an inertia element is displaced from its equilibrium position due to an energy imparted to the system through an external source. Vibrations in many engineering systems can lead to catastrophic situations and dangerous accidents if uncontrolled. Therefore, vibration reduction, control, and stabilization of dynamical systems are quite important problems. Various techniques of vibration reduction, control, and some time suppression are developed to channel the excess energy from the excited system to a slave one. One of the most feasible vibration reduction methods is the saturation phenomenon based technique that has been discovered by Nayfeh et al. [1]. They reported that in the case of quadratic coupling nonlinearities the energy transfer is complete if the natural frequencies of the main system and the secondary system are in the ratio two to one. The saturation phenomenon has been the subject of extensive theoretical and experimental research [2,3,4,5,6]. One of the passive vibration absorbers that works based on the saturation phenomenon is the autoparametric vibration absorber. The main structure of such system lies in attaching absorber (pendulum) to the primary system (oscillator) in a way such that the pendulum is exposed to a parametric

base excitation of the primary system. Autoparametric systems consist of two nonlinear subsystems coupled to interact in a way so that one of them (high natural frequency subsystem) transfers the exogenous energy parametrically to the other (low natural frequency subsystem). Warminski et al. [7,8,9,10,11] discussed autoparametric system consists of a nonlinear oscillator with an attached pendulum. In Ref. [7] they derived the system equations of motion. The model showed that the system is strongly nonlinear and the motions of both subsystems are strongly coupled by inertial terms leading to the so-called autoparametric vibration. An approximate analytical solution of the system model is obtained applying the harmonic balance method [8]. The influence of some essential parameters on the system stability is discussed in Ref. [9]. In Ref. [10], the authors studied the vibration control of Duffing oscillator mounted on magnetorheological (MR) damper and nonlinear spring attached to pendulum. Warminski et al. [11] studied vibration analysis of an autoparametric pendulum-like mechanism subjected to harmonic excitation. They proposed a suspension composed of a semi-active MR damper and a nonlinear spring. Kecik [12] studied the nonlinear oscillations of autoparametric system consists of a nonlinear oscillator attached to pendulum system. A combination of MR damper together with a nonlinear

* Corresponding author e-mail: wedad.ali.el.ganaini@gmail.com

spring made from a shape memory alloy is proposed. He concluded that it is possible to fit on-line the structure response to the frequency and amplitude of external excitation. Brzeski et al. [13] studied the dynamics of the pendulum suspended on forced Duffing oscillator. The detailed bifurcation analysis in two-parameter space has been performed. They found too large ranges of the parameters space have only one attractor around 1:1 principal resonance in neighborhood of 2: 1 internal resonance. Refs [14,15,16,17,18] studied the same model with different analytical techniques. In Refs [19, 20,21] the pendulum is studied as a nonlinear vibration absorber attached to a horizontally moving Duffing oscillator at 1:1 internal resonance and 1:1 principal parametric resonance. Tusset et al. [22] studied the chaotic behaviors control of parametrically excited pendulum using two different control strategies. One of this applied control method is via the active nonlinear saturation controller, and the other via introducing a passive rotational MR damper. Within this paper, a detailed analysis for a vertically moving Duffing oscillator attached pendulum has been introduced. Based on the results obtained in Ref. [13], the 1:2 internal resonance case is studied when the oscillator is excited periodically near its natural frequency (primary resonance). The system amplitude-phase modulating equations are extracted applying the multiple scales perturbation technique. The frequency-response curves before and after linking the absorber to the system are obtained. The effects of the coupling parameters, absorber linear damping coefficient, and excitation amplitude on the frequency-response curve are explored. Numerical confirmations for the all acquired results are performed. Time-histories are conducted to show the exchange of energy between the two subsystems (i.e. the Duffing oscillator and the pendulum). Finally, important notes are included for the optimal working conditions and design of such system.

2 System model and Perturbation analysis

The considered system consists of a pendulum suspended on the Duffing oscillator, where the oscillator is excited periodically in the vertical direction as shown in Fig.1. The system dimensionless equations of motions are given as follows [7, 8]

$$\ddot{y} + \mu_1 \dot{y} + \omega_1 y + \beta_1 y^3 = \gamma \cos(\Omega t) - \alpha_1 (\ddot{\theta} \sin \theta + \dot{\theta}^2 \cos \theta) \quad (1)$$

$$\ddot{\theta} + \mu_2 \dot{\theta} + \theta = -\alpha_2 \ddot{y} \sin \theta \quad (2)$$

List of symbols: y, \dot{y}, \ddot{y} Displacement, velocity, and acceleration of the Duffing oscillator system, respectively. $\theta, \dot{\theta}, \ddot{\theta}$ Displacement, velocity, and acceleration of the

pendulum inclination angle, respectively. μ_1, μ_2 Linear damping coefficients of the Duffing oscillator system and pendulum, respectively. ω_1 Linear natural frequency of the Duffing oscillator system. β_1, β_2 The system nonlinear stiffness coefficients. α_1, α_2 The system nonlinear coupling coefficients. Ω, γ External excitation frequency and external excitation amplitude, respectively.

Replacing the nonlinear functions $\sin \theta$ and $\cos \theta$ in equations (1) and (2) by their third-order approximating Taylor series, yields:

$$\ddot{y} + \mu_1 \dot{y} + \omega_1^2 y + \beta_1 y^3 = \gamma \cos(\Omega t) + \alpha_1 \left(\frac{1}{2} \dot{\theta}^2 \theta^2 + \frac{1}{6} \ddot{\theta} \theta^3 - \dot{\theta}^2 - \ddot{\theta} \theta \right) \quad (3)$$

$$\ddot{\theta} + \mu_2 \dot{\theta} + \theta - \beta_2 \theta^3 = \alpha_2 \left(\frac{1}{6} \ddot{y} \theta^3 - \dot{y} \theta \right) \quad (4)$$

Applying the multiple scales perturbation method [23], we can obtain a first-order approximate solution to equations (3) and (4) by seeking the solution as:

$$y(t, \varepsilon) = y_1(T_0, T_1) + \varepsilon y_2(T_0, T_1) + O(\varepsilon^2) \quad (5)$$

$$\theta(t, \varepsilon) = \theta_1(T_0, T_1) + \varepsilon \theta_2(T_0, T_1) + O(\varepsilon^2) \quad (6)$$

where ε is a small dimensionless perturbation parameter used for book-keeping only, $T_0 = t$ and $T_1 = \varepsilon t$ are the fast and slow time scales, respectively. In terms of T_0 and T_1 the time derivatives can be expressed using the chain rule as:

$$\frac{d}{dt} = D_0 + \varepsilon D_1, \quad \frac{d^2}{dt^2} = D_0^2 + 2\varepsilon D_0 D_1, \\ \text{where } D_j = \frac{\partial}{\partial T_j}, \quad j = 0, 1 \quad (7)$$

To make damping, nonlinearities, and the excitation force appear in the same perturbed equation, the system parameters have to be scaled as follows:

$$\mu_n = \varepsilon \hat{\mu}_n, \quad \beta_n = \varepsilon \hat{\beta}_n, \quad \alpha_n = \varepsilon \hat{\alpha}_n, \quad \gamma = \varepsilon \hat{\gamma}; \quad n = 1, 2 \quad (8)$$

Substituting equations (5) to (8) into equations (3) and (4), and equating coefficients of like powers of ε , we get the following set of differential equations:

$$O(\varepsilon^0): \\ (D_0^2 + \omega_1^2) y_1 = 0 \quad (9)$$

$$(D_0^2 + 1) \theta_1 = 0 \quad (10)$$

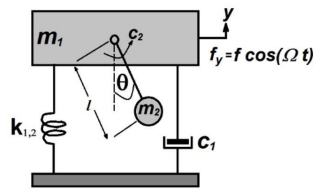


Fig. 1: System model

$O(\varepsilon^1)$:

$$(D_0^2 + \omega_1^2)y_2 = -2D_0D_1y_1 - \hat{\mu}_1D_0y_1 - \hat{\beta}_1y_1^3 - \hat{\alpha}_1 \left(\left(1 - \frac{1}{6}\theta_1^2\right)\theta_1D_0^2\theta_1 + \left(1 - \frac{1}{2}\theta_1^2\right)(D_0\theta_1)^2 \right) + \hat{\gamma}\cos(\Omega t) \tag{11}$$

$$(D_0^2 + 1)\theta_2 = -2D_0D_1\theta_1 - \hat{\mu}_2D_0\theta_1 + \hat{\beta}_2\theta_1^3 - \hat{\alpha}_2 \left(\left(1 - \frac{1}{6}\theta_1^2\right)\theta_1D_0^2y_1 \right) \tag{12}$$

The solution of equations (9) and (10), can be expressed as

$$y_1(T_0, T_1) = A(T_1)e^{i\omega_1 T_0} + cc \tag{13}$$

$$\theta_1(T_0, T_1) = B(T_1)e^{iT_0} + cc \tag{14}$$

where cc denotes the complex conjugate of the preceding terms. Inserting equations (13) and (14) into equations (11) and (12), we have

$$(D_0^2 + \omega_1^2)y_2 = (-2i\omega_1D_1A - i\hat{\mu}_1\omega_1A - 3\hat{\beta}_1A^2\bar{A})e^{i\omega_1T_0} - \hat{\beta}_1A^3e^{3i\omega_1T_0} + 2\hat{\alpha}_1B^2\left(1 - \frac{1}{3}B\bar{B}\right)e^{2iT_0} - \frac{2}{3}\hat{\alpha}_1B^4e^{4iT_0} + \frac{\hat{\gamma}}{2}e^{i\Omega T_0} + cc \tag{15}$$

$$(D_0^2 + 1)\theta_2 = (-2iD_1B - i\hat{\mu}_2B + 3\hat{\beta}_2B^2\bar{B})e^{iT_0} + \hat{\beta}_2B^3e^{3iT_0} - \frac{1}{6}\hat{\alpha}_2\omega_1^2AB^3e^{i(\omega_1+3)T_0} - \hat{\alpha}_2\omega_1^2AB\left(\frac{1}{2}B\bar{B} - 1\right)e^{i(\omega_1+1)T_0} - \hat{\alpha}_2\omega_1^2A\bar{B}\left(\frac{1}{2}B\bar{B} - 1\right)e^{i(\omega_1-1)T_0} - \frac{1}{6}\hat{\alpha}_2\omega_2^2A\bar{B}^3e^{i(\omega_1-3)T_0} + cc \tag{16}$$

The deduced resonance conditions from equations (15) and (16) are the primary resonance ($\Omega = \omega_1$), internal resonance ($\omega_1 = 2, \omega_1 = 4$), and simultaneous

resonance ($\Omega = \omega_1 = 2, \Omega = \omega_1 = 4$). In this paper, the simultaneous resonances case ($\Omega = \omega_1 = 2$) is considered. So, the closeness of the considered resonances can be described quantitatively by introducing the detuning parameters σ_1 and σ_2 according to:

$$\omega_1 = 2 + \sigma_1 = 2 + \varepsilon\hat{\sigma}_1, \quad \Omega_1 = 2 + \sigma_2 = 2 + \varepsilon\hat{\sigma}_2 \tag{17}$$

Inserting equations (17) into secular and the small-divisor terms in equations (15) and (16), we get

$$(D_0^2 + \omega_1^2)y_2 = (-2i\omega_1D_1A - i\hat{\mu}_1\omega_1A - 3\hat{\beta}_1A^2\bar{A})e^{i\omega_1T_0} - \hat{\beta}_1A^3e^{3i\omega_1T_0} + 2\hat{\alpha}_1B^2\left(1 - \frac{1}{3}B\bar{B}\right)e^{-i\hat{\sigma}_1T_1}e^{i\omega_1T_0} - \frac{2}{3}\hat{\alpha}_1B^4e^{4iT_0} + \frac{\hat{\gamma}}{2}e^{i(\hat{\sigma}_2 - \hat{\sigma}_1)T_1}e^{i\omega_1T_0} + cc \tag{18}$$

$$(D_0^2 + 1)\theta_2 = (-2iD_1B - i\hat{\mu}_2B + 3\hat{\beta}_2B^2\bar{B})e^{iT_0} + \hat{\beta}_2B^3e^{3iT_0} - \frac{1}{6}\hat{\alpha}_2\omega_1^2AB^3e^{i(\omega_1+3)T_0} - \hat{\alpha}_2\omega_1^2AB\left(\frac{1}{2}B\bar{B} - 1\right)e^{i(\omega_1+1)T_0} - \hat{\alpha}_2\omega_1^2A\bar{B}\left(\frac{1}{2}B\bar{B} - 1\right)e^{i\hat{\sigma}_1T_1}e^{iT_0} - \frac{1}{6}\hat{\alpha}_2\omega_1^2A\bar{B}^3e^{-i\hat{\sigma}_1T_1}e^{iT_0} + cc \tag{19}$$

The solvability conditions of equations (18) and (19) are

$$-2i\omega_1D_1A - i\hat{\mu}_1\omega_1A - 3\hat{\beta}_1A^2\bar{A} + 2\hat{\alpha}_1B^2\left(1 - \frac{1}{3}B\bar{B}\right)e^{-i\hat{\sigma}_1T_1} + \frac{\hat{\gamma}}{2}e^{i(\hat{\sigma}_2 - \hat{\sigma}_1)T_1} = 0 \tag{20}$$

$$-2iD_1B - i\hat{\mu}_2B + 3\hat{\beta}_2B^2\bar{B} - \hat{\alpha}_2\omega_1^2A\bar{B}\left(\frac{1}{2}B\bar{B} - 1\right)e^{i\hat{\sigma}_1T_1} - \frac{1}{6}\hat{\alpha}_2\omega_1^2A\bar{B}^3e^{-i\hat{\sigma}_1T_1} = 0 \tag{21}$$

To analyze the solutions of equations (20) and (21), we let

$$A(T_1) = \frac{1}{2}\alpha_1(T_1)e^{i\lambda_1(T_1)}, \quad B(T_1) = \frac{1}{2}\alpha_2(T_1)e^{i\lambda_2(T_1)} \tag{22}$$

where α_1 and α_2 are the steady-state amplitudes of Duffing oscillator and pendulum, respectively, λ_1 and λ_2 are the phases of the two motions. Inserting equations (22) into (20) and (21) with separating the real and imaginary parts, we get the flowing amplitude-phase modulating equations governing the system dynamics.

$$\dot{a}_1 = -\frac{1}{2}\mu_1 a_1 - \frac{1}{2\omega_1}\alpha_1 a_2^2 \left(1 - \frac{1}{12}a_2^2\right) \sin(\varphi_2) - \frac{\gamma}{2\omega_1} \sin(\varphi_1), \tag{23.a}$$

$$\begin{aligned} \dot{\varphi}_1 &= \sigma_1 - \sigma_2 + \frac{3}{8\omega_1}\beta_1 a_1^2 - \frac{1}{2\omega_1 a_1}\alpha_1 a_2^2 \left(1 - \frac{1}{12}a_2^2\right) \cos(\varphi_2) \\ &\quad - \frac{\gamma}{2\omega_1 a_1} \cos(\varphi_1), \end{aligned} \tag{23.b}$$

$$\dot{a}_2 = -\frac{1}{2}\mu_2 a_2 + \frac{1}{4}\alpha_2 \omega_1^2 a_1 a_2 \left(1 - \frac{1}{12}a_2^2\right) \sin(\varphi_2), \tag{23.c}$$

$$\begin{aligned} \dot{\varphi}_2 &= \sigma_1 + \frac{3}{8\omega_1}\beta_1 a_1^2 + \frac{3}{4}\beta_2 a_2^2 - \frac{\gamma}{2\omega_1 a_1} \cos(\varphi_1) \\ &\quad - \frac{1}{2\omega_1 a_1}\alpha_1 a_2^2 \left(1 - \frac{1}{12}a_2^2\right) \cos(\varphi_2) \\ &\quad - \alpha_2 \omega_1^2 a_1 \left(\frac{1}{12}a_2^2 - \frac{1}{2}\right) \cos(\varphi_2). \end{aligned} \tag{23.d}$$

where $\varphi_1 = \lambda_1 - (\sigma_2 - \sigma_1)t$ and $\varphi_2 = \lambda_1 - 2\lambda_2 + \sigma_1 t$. At steady-state oscillations, we have $\dot{a}_1 = \dot{a}_2 = \dot{\varphi}_1 = \dot{\varphi}_2 = 0$, substituting this conditions into equations (23), we get

$$\mu_1 a_1 + \frac{1}{\omega_1}\alpha_1 a_2^2 \left(1 - \frac{1}{12}a_2^2\right) \sin(\varphi_2) + \frac{\gamma}{\omega_1} \sin(\varphi_1) = 0 \tag{24.a}$$

$$\begin{aligned} \sigma_1 - \sigma_2 + \frac{3}{8\omega_1}\beta_1 a_1^2 \\ - \frac{1}{2\omega_1 a_1}\alpha_1 a_2^2 \left(1 - \frac{1}{12}a_2^2\right) \cos(\varphi_2) \\ - \frac{\gamma}{2\omega_1 a_1} \cos(\varphi_1) = 0 \end{aligned} \tag{24.b}$$

$$\mu_2 a_2 - \frac{1}{2}\alpha_2 \omega_1^2 a_1 a_2 \left(1 - \frac{1}{12}a_2^2\right) \sin(\varphi_2) = 0 \tag{24.c}$$

$$\begin{aligned} \sigma_1 + \frac{3\beta_1}{8\omega_1} a_1^2 + \frac{3\beta_2}{4} a_2^2 - \frac{\gamma}{2\omega_1 a_1} \cos(\varphi_1) \\ - \frac{\alpha_1}{2\omega_1 a_1} a_2^2 \left(1 - \frac{1}{12}a_2^2\right) \cos(\varphi_2) \\ - \alpha_2 \omega_1^2 a_1 \left(\frac{1}{12}a_2^2 - \frac{1}{2}\right) \cos(\varphi_2) = 0 \end{aligned} \tag{24.d}$$

The performance of the pendulum as a passive vibration absorber can be evaluated by solving the nonlinear algebraic equations (24) numerically in terms of $\sigma_1, \sigma_2, \alpha_1, \alpha_2, \beta_1, \mu_2$ and γ .

3 Steady state solution stability

The stability of the equilibrium solution is determined by examining the Jacobian matrix eigenvalues of the right-hand sides of equations (23). To derive the stability criteria, we need to examine the behavior of small perturbation from the steady-state solution ($\alpha_{10}, \alpha_{20}, \varphi_{10}$ and φ_{20}) of equations (24). Thus, we assume that

$$\begin{aligned} a_1 &= a_{11} + a_{10}, \quad a_2 = a_{21} + a_{20}, \\ \varphi_1 &= \varphi_{11} + \varphi_{10}, \quad \varphi_2 = \varphi_{21} + \varphi_{20} \\ \dot{a}_1 &= \dot{a}_{11}, \quad \dot{a}_2 = \dot{a}_{21}, \quad \dot{\varphi}_1 = \dot{\varphi}_{11}, \quad \dot{\varphi}_2 = \dot{\varphi}_{21} \end{aligned} \tag{25}$$

where $\alpha_{11}, \alpha_{21}, \varphi_{11}$ and φ_{21} are perturbations, which are assumed to be small compared to the assumed steady state solution ($\alpha_{10}, \alpha_{20}, \varphi_{10}$ and φ_{20}). Substituting equations (25) into equations (23), and expanding for small $\alpha_{11}, \alpha_{21}, \varphi_{11}$ and φ_{21} and keeping linear terms only, we get

$$\begin{bmatrix} \dot{a}_{11} \\ \dot{\varphi}_{11} \\ \dot{a}_{21} \\ \dot{\varphi}_{21} \end{bmatrix} = \begin{bmatrix} r_{11} & r_{12} & r_{13} & r_{14} \\ r_{21} & r_{22} & r_{23} & r_{24} \\ r_{31} & r_{32} & r_{33} & r_{34} \\ r_{41} & r_{42} & r_{43} & r_{44} \end{bmatrix} \begin{bmatrix} a_{11} \\ \varphi_{11} \\ a_{21} \\ \varphi_{21} \end{bmatrix} \tag{26}$$

where the above matrix represents the system Jacobian matrix. Thus, the stability of the steady-state motion depends on the eigenvalues of Jacobian matrix. One can obtain the following eigenvalue equation

$$\delta^4 + \zeta_1 \delta^3 + \zeta_2 \delta^2 + \zeta_3 \delta + \zeta_4 = 0 \tag{27}$$

where δ denotes eigenvalues of Jacobian matrix, $\zeta_1, \zeta_2, \zeta_3$ and ζ_4 are coefficients of equation (27). According to Routh-Hurwitz criterion, the necessary and sufficient conditions for stable system are

$$\zeta_1 > 0, \quad \zeta_1 \zeta_2 - \zeta_3 > 0, \quad \zeta_3(\zeta_1 \zeta_2 - \zeta_3) - \zeta_1^2 \zeta_4 > 0, \quad \zeta_4 > 0. \tag{28}$$

4 Results and discussions

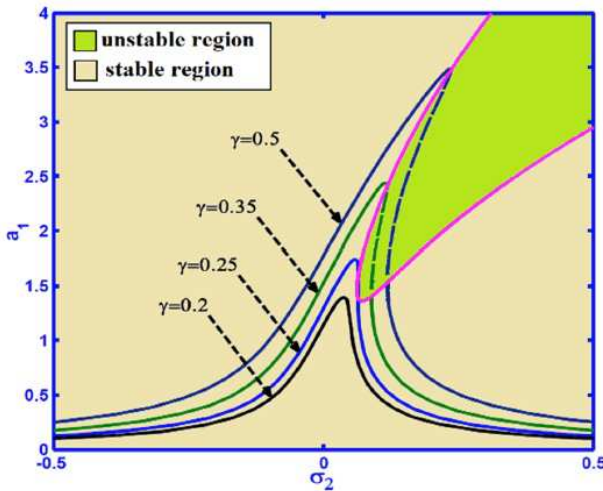


Fig. 2: Duffing oscillator frequency-response curves at different values of the excitation amplitude γ

The considered system is investigated at different values of its parameters. The obtained results are presented in graphical forms as steady-state amplitudes against detuning parameter σ_2 and the excitation amplitude γ . The system is analyzed at the parameters values: $\mu_1 = 0.0716, \mu_2 = 0.0202, \omega_1 = 2, \alpha_1 = 0.3636, \alpha_2 = 0.25, \beta_1 = 0.1031, \beta_2 = 0.1666, \sigma_1 = \sigma_2 = 0.0$ and $\gamma = 0.1$ unless otherwise specified [7-13]. The bifurcation diagrams were plotted as solid lines correspond to stable solutions, and as dashed lines correspond to unstable ones. To validate the accuracy of the analytical results, the original equations (1) and (2) have been integrated numerically using the slandered Matlab solver **ODE45**. The obtained numerical results were shown as small circles at the initial conditions $y(0) = \dot{y}(0) = \dot{\theta}(0) = 0, \theta(0) = 0.1$ and as big-dots at the initial conditions $y(0) = \dot{y}(0) = \dot{\theta}(0) = 0, \theta(0) = -\frac{\pi}{2}$. Fig. 2 shows Duffing oscillator frequency-response curves when exposed to various levels of excitation amplitude γ . It is clear from the figure that as the excitation amplitude increases the response-curve bend to the right leading to jump phenomenon occurrence and the nonlinearity dominates the response. Fig. 3 shows the controlled system frequency-response curve at $\gamma = 0.1$. The response amplitude depends on σ_2 and the initial conditions, whereas σ_2 increases gradually from a large negative value, the absorber remains at static equilibrium (trivial solution), while the oscillator vibrates with small amplitude until σ_2 reaches point B, beyond this point there are two possible stable solutions, where the system will follow one of them based on the its initial conditions. If the initial conditions are small, the system will trace the

curve B-E until σ_2 reaches point E. At point E, the absorber loses the stability of its trivial solution through a transcritical bifurcation and the resulting non-trivial solution encounters a saddle-node bifurcation, leading to jumping up to the point D. Further increasing of σ_2 , the system amplitude traces the curve D-F-K-G. when σ_2 reaches point G, the solution encounters a saddle-node bifurcation leading to jumping to point H, where the trivial solution of the absorber is reached again. If the initial conditions are large, the system will trace the A-B-C-D-F-K-G-H-I path. As σ_2 decreases gradually from a large positive value the absorber remains in static equilibrium with the trivial solution, while the oscillator vibrates at small amplitude until σ_2 reaches point H. After σ_2 crossing the point H, there are two possible solutions. If the initial conditions are small the system response will trace the curve H-J. When J is reached, the absorber loses the stability of its trivial solution through a transcritical bifurcation and the resulting non-trivial solution encounters a saddle-node bifurcation leading to a jump to point K. Further decreasing of σ_2 , the system amplitude traces the curve F-D until point C is reached, at that point C, the solution encounters a saddle-node bifurcation leading to a jump to point B, where the trivial solution of the absorber is reached. If the initial conditions are large the system will trace the I-H-G-K-F-D-C-B-A path. The figure also verifies a good agreement between the obtained analytical solutions and the numerical simulations of the original equations (1) and (2). Fig. 4 shows the system time histories according to point P_1 that marked on Fig. 3 (i.e. at $\sigma_2 = 0.0, \gamma = 0.1$). It can be seen from the figure that the vibrations are transferred parametrically from the oscillator to the absorber. The numerical solution of equations (23) for the chosen values of the system parameters is presented graphically in Fig. 4. The dashed lines show the modulation of the amplitudes for the generalized coordinates y and θ . The simulation results show that equations (23) describe with high accuracy not only the steady-state modulating amplitudes, but also the transient modulating amplitudes of the whole system. The time histories of the system according to points P_2 and P_3 that marked on Fig. 3 are shown in Fig. 5. It is noticed that the system parameters according to the two points P_2 and P_3 are the same, but the initial conditions of the pendulum are changed from $\theta(0) = -\frac{\pi}{2}$ to $\theta(0) = 0.1$, whereas other initial conditions remain zeros. The figure confirms the sensitivity of the system to the initial conditions. In Fig. 6, we illustrate the force-response curves of both Duffing oscillator and pendulum at four different values of σ_2 . We can trace the histories of both α_1 and α_2 when the excitation amplitude γ is slowly increased beyond zero. Initially, both α_1 and α_2 are zeros and they follow the curve according to the value of σ_2 . Fig. 6a shows that at $\sigma_2 = 0$ the oscillator steady-state amplitude increases as the excitation force amplitude increases until γ reaches a critical value, while the absorber steady-state amplitude remains zero. Beyond this critical value the oscillator

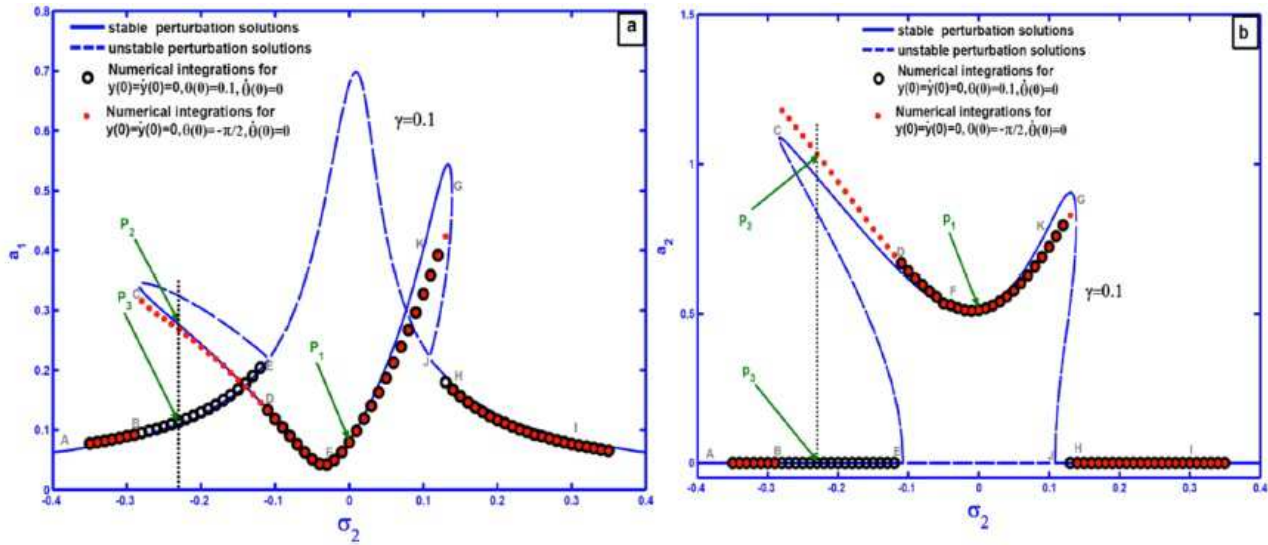


Fig. 3: System frequency-response curves: (a) Duffing oscillator, and (b) pendulum, at $\gamma = 0.1$, the circles denote the numerical solutions according to initial conditions $y(0) = \dot{y}(0) = \theta(0) = 0, \theta(0) = 0.1$, while the big-dots represent the numerical solutions according to initial conditions $y(0) = \dot{y}(0) = \theta(0) = 0, \theta(0) = -\frac{\pi}{2}$.

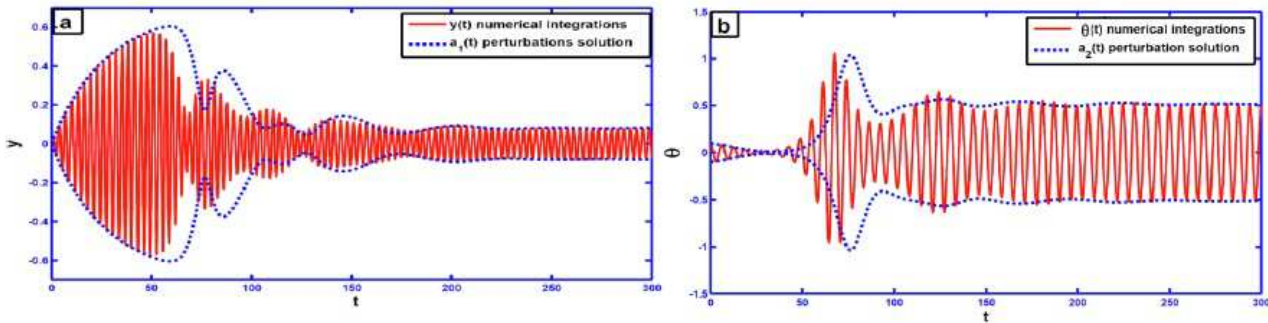


Fig. 4: System time-histories according to point P_1 that marked on Fig. 3: (a) Duffing oscillator, and (b) pendulum

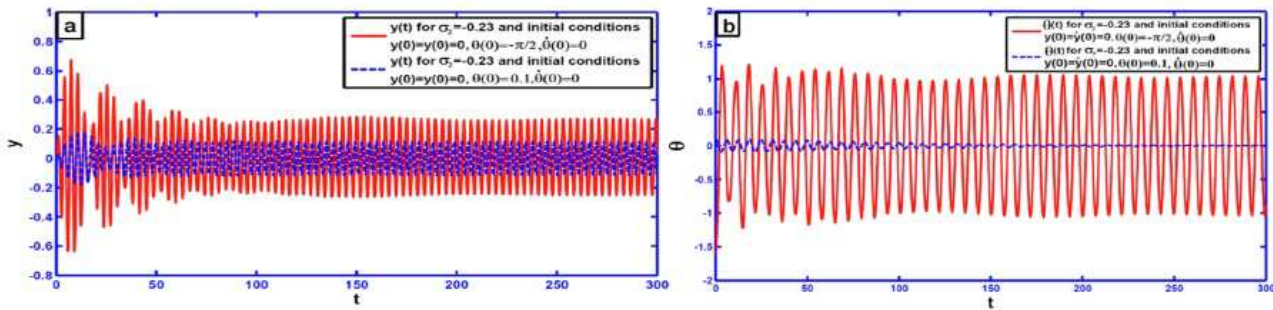


Fig. 5: System time-histories according to points P_2 and P_3 that illustrated in Fig. 3: (a) Duffing oscillator, and (b) pendulum

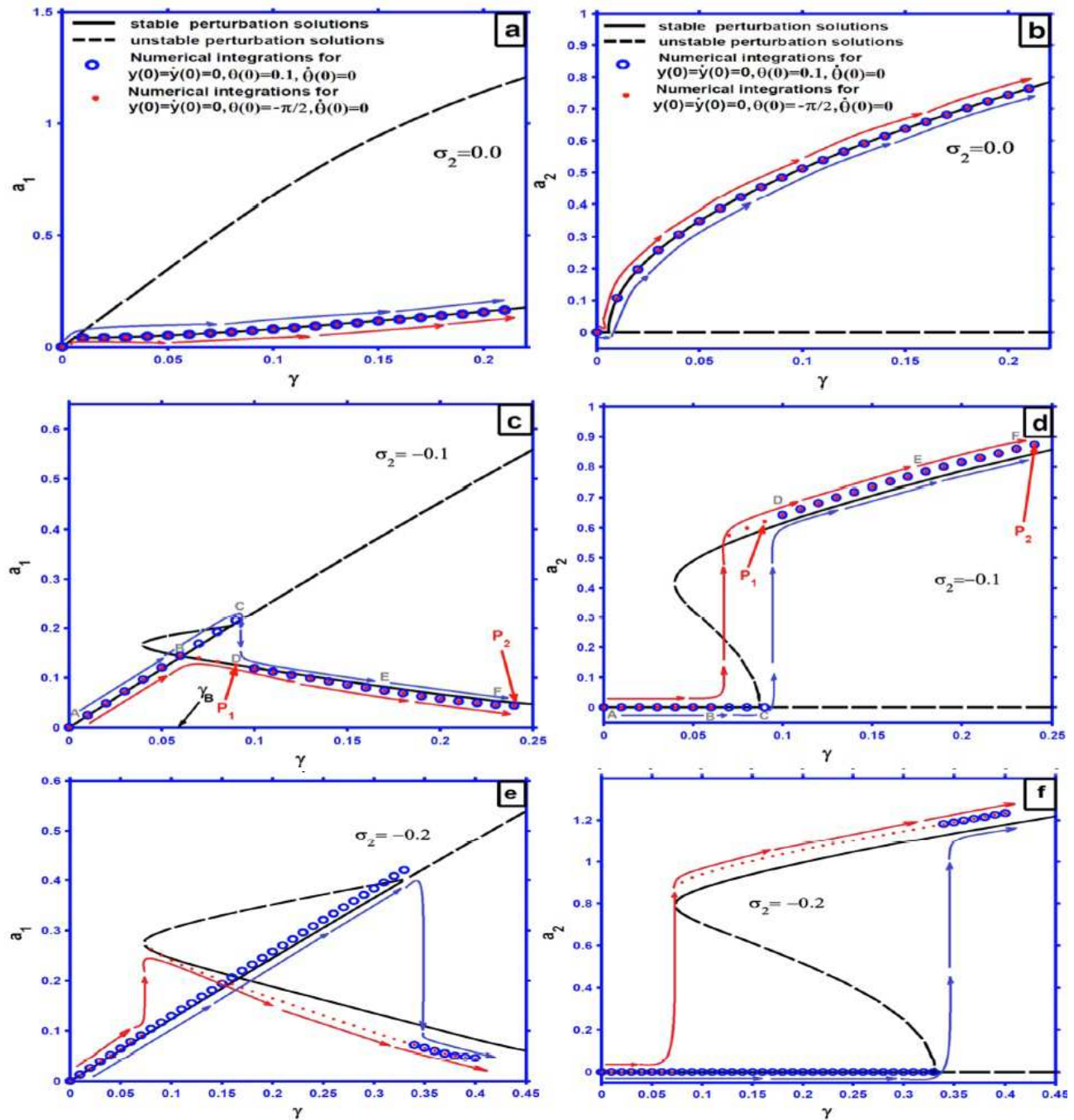


Fig. 6: Effect of varying the external detuning parameter σ_2 on the force-response curves: Duffing oscillator (left column), and pendulum (right column)

steady-state amplitude saturates to a constant value and all excessive energy due to excitation force is channeled to the pendulum as shown in Fig. 6b. In addition, the figure shows that the system motion is independent of the initial conditions. Figs. 6c and 6d show the force-response curves at $\sigma_2 = -0.1$. It is clear that the

amplitude of the response depends on γ magnitude and the system initial conditions. For $\gamma < \gamma_B$, the absorber remains in static equilibrium, while the oscillator vibrates at small amplitude, but when γ exceeds γ_B , there are two possible solutions and the system follows one of them based on the initial conditions. If the initial conditions are

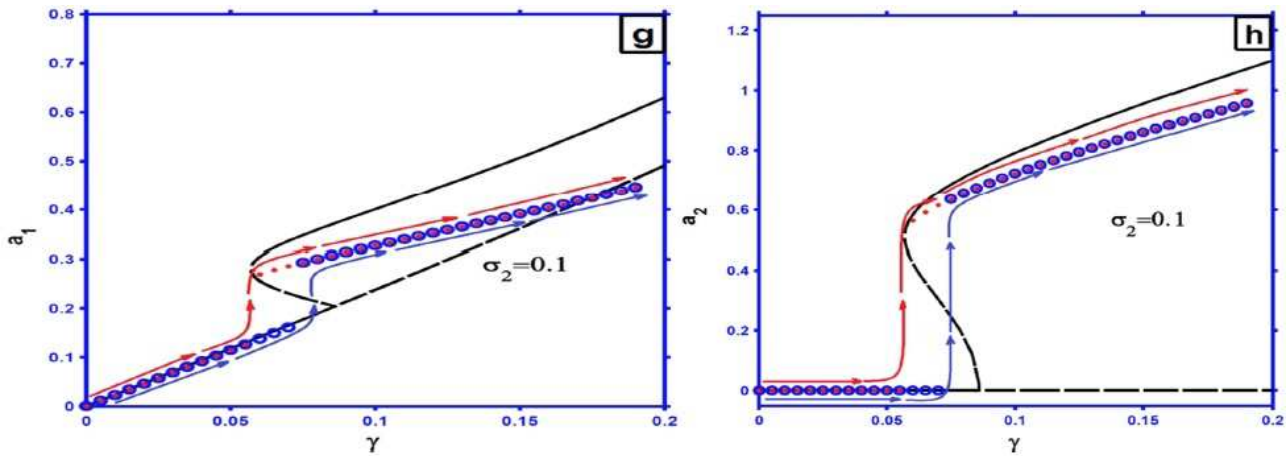


Fig. 6: (continued)

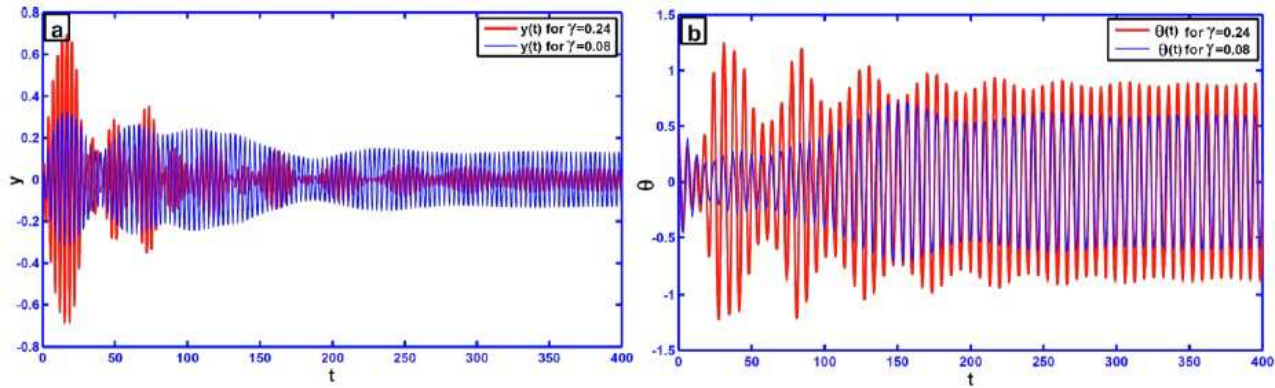


Fig. 7: System time-histories according to points P_1 (i.e. $\sigma_2 = -0.1, \gamma = 0.08$) and P_2 ($\sigma_2 = -0.1, \gamma = 0.24$) that marked on Fig. 6: (a) Duffing oscillator, and (b) pendulum

small the system traces the curve A-B-C. When reaching point C, the absorber loses its trivial solution through a transcritical bifurcation and the resulting non-trivial solution encounters a saddle-node bifurcation leading to a jump to point D. Upon further increasing of γ the system amplitude traces the curve D-E-F. If the initial conditions are large the system will trace A-B-D-E-F path. Figs. 6e and 6f show the system force-response curve when $\sigma_2 = -0.2$ while Figs. 6g and 6h show the system force-response curve at $\sigma_2 = 0.1$. Fig. 7 shows the time histories for both the oscillator and pendulum displacements according to points P_1 and P_2 that marked on Fig. 6. The influence of the nonlinear parameter α_1 on the system frequency-response curve is presented in Fig. 8. The figure shows that as α_1 increases both the oscillator and the pendulum steady state amplitudes decrease without observable effect on the pendulum bandwidth. Fig. 9 shows the time histories according to points P_1, P_2 , and P_3 that marked on Fig. 8. In Fig. 10, we show the influence of α_2 on the system

frequency-response curve. Increasing α_2 , decreases both the oscillator and pendulum steady state amplitudes and increases the pendulum active bandwidth. The time histories for both the oscillator and pendulum according to points P_1 and P_2 that marked on Fig. 10 are shown in Fig. 11. Fig. 12 shows the effect of the pendulum linear damping coefficient μ_2 on the frequency-response curve of the system. It is noted that decreasing μ_2 decreases the oscillator steady-state amplitude and increases the pendulum steady-state amplitude. Fig. 13 and 14 show the time histories according to points P_1 and P_2 that marked on Fig. 12, where Fig. 13 was plotted at initial conditions $y(0) = \dot{y}(0) = \dot{\theta}(0) = 0, \theta(0) = 0.1$ and Fig. 14 was plotted at initial conditions $y(0) = \dot{y}(0) = \dot{\theta}(0) = 0, \theta(0) = -\frac{\pi}{2}$. It is clear from both figures that the energy transfer from the oscillator to the pendulum increases as μ_2 decreases. However, changing the initial conditions affect only the transient response of the system.

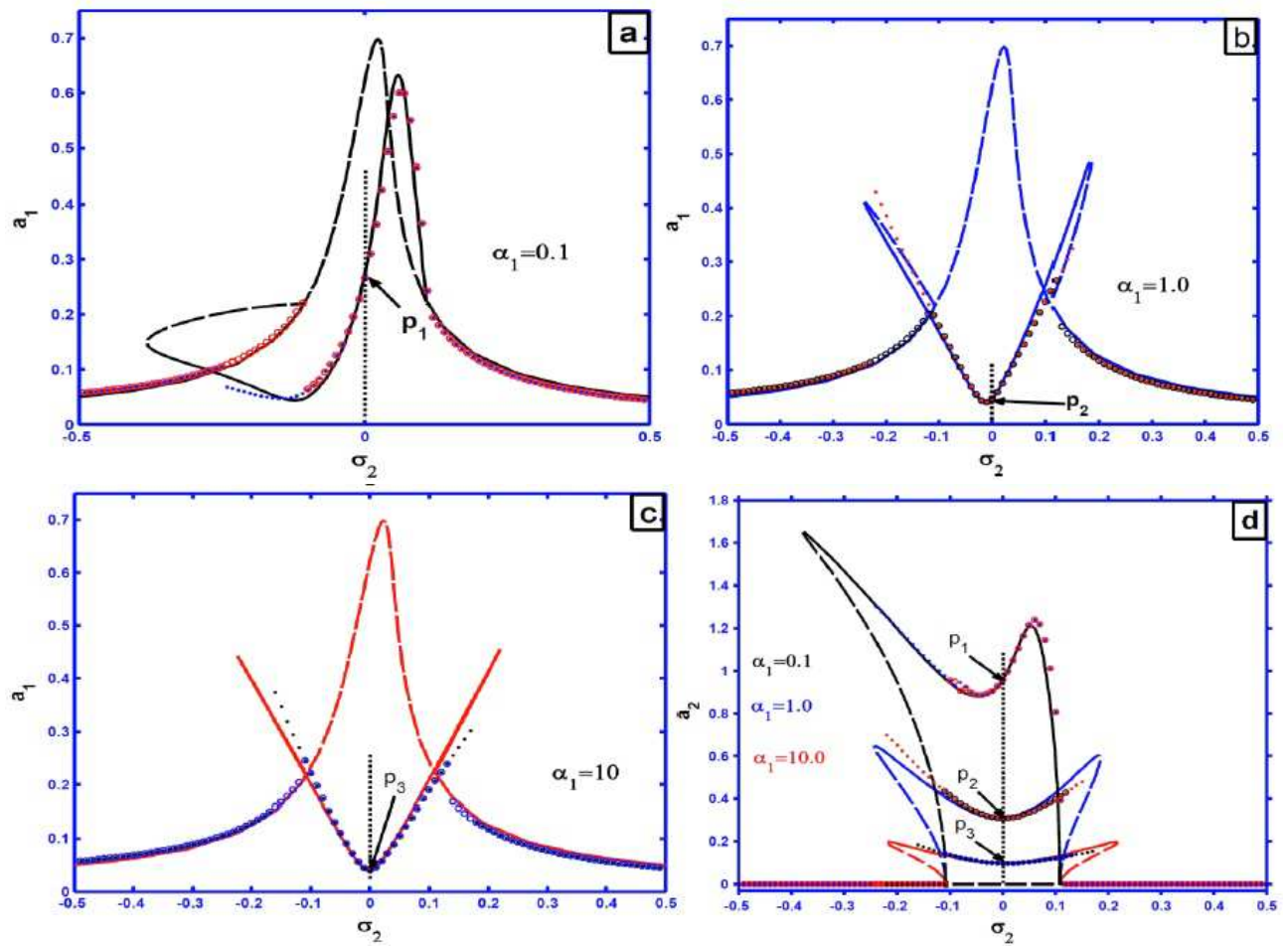


Fig. 8: Effect of increasing the nonlinear parameters α_1 on the system frequency-response curves: (a, b, c) Duffing oscillator, and (d) pendulum

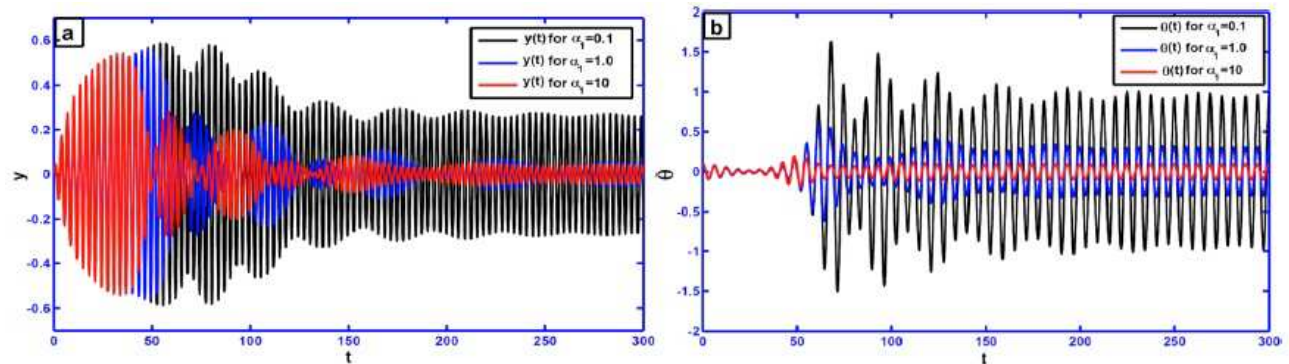


Fig. 9: System time-histories according to point P_1 , P_2 , and P_3 that illustrated in Fig. 8: (a) Duffing oscillator, and (b) pendulum

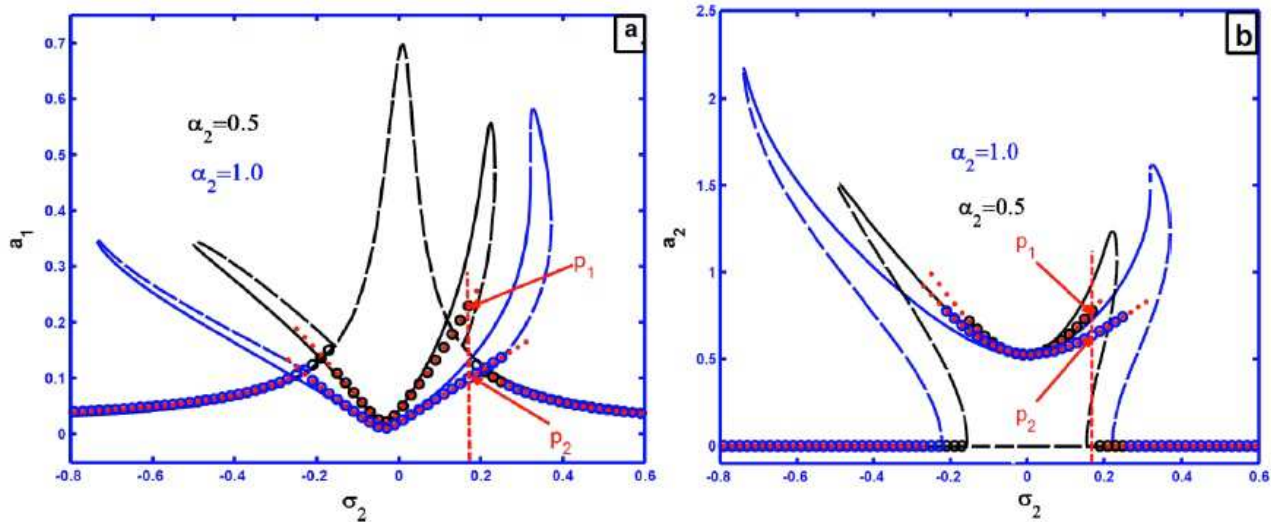


Fig. 10: Effect of increasing the nonlinear parameters α_2 on the frequency-response curves: (a) Duffing oscillator, and (b) pendulum.

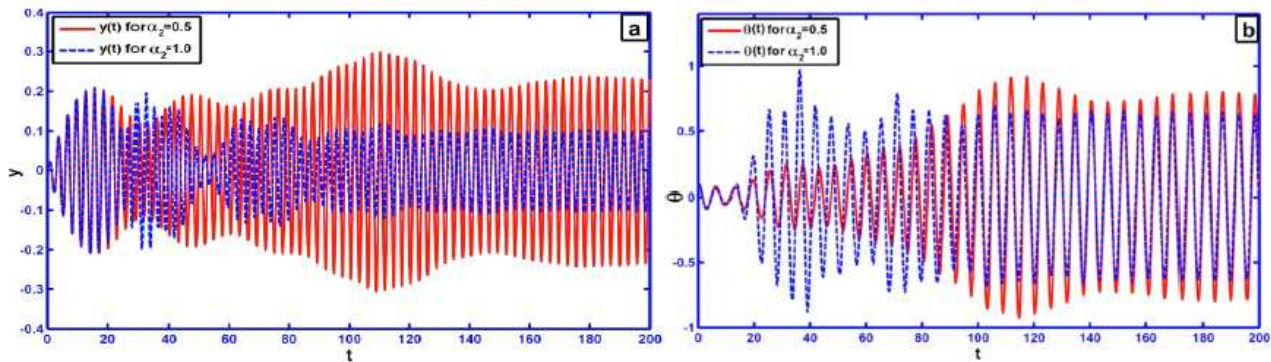


Fig. 11: System Time-histories according to point P_1 ($\sigma_2 = 0.17, \alpha_2 = 0.5$), and P_2 ($\sigma_2 = 0.17, \alpha_2 = 1.0$) that marked on Fig. 10: Duffing oscillator, and (b) pendulum.

5 Conclusions

1. At perfect external tuning (i.e. $\sigma_2 = 0$), the saturation phenomenon occurs and the Duffing oscillator vibration amplitude saturates to a very small value, while all excessive vibrational energy of the oscillator due to increasing of the excitation amplitude is pumped to the pendulum parametrically.
2. At negative external detuning (i.e. $-0.2 \leq \sigma_2 < 0$), increasing the excitation force amplitude (γ), increases vibration amplitude of Duffing oscillator until γ reaches a critical value, beyond this value the Duffing oscillator vibration amplitude decreases as γ increases.
3. At positive external detuning (i.e. $0 < \sigma_2 \leq 0.1$), increasing the excitation force amplitude (γ), increases the oscillator vibration amplitude until γ

reaches a critical value, beyond this value the pendulum adds more vibrational energy to the oscillator instead of absorbing it. Accordingly, the occurrence of positive detuning must be avoided in the design of such systems.

In comparison with previous work [7,8,9,10,11,12], the authors discussed an autoparametric system consists of a nonlinear oscillator attached to pendulum system. They obtained an approximate analytical solution for the system equations of motion using harmonic balance method. The influence of some essential parameters on the system stability is studied. In [10] they studied the vibration control of Duffing oscillator mounted on magnetorheological (MR) damper and nonlinear spring attached to a pendulum. They concluded that the control methods allow the system to maintain on the desirable attractor. Warminski et al. [11] studied vibration analysis

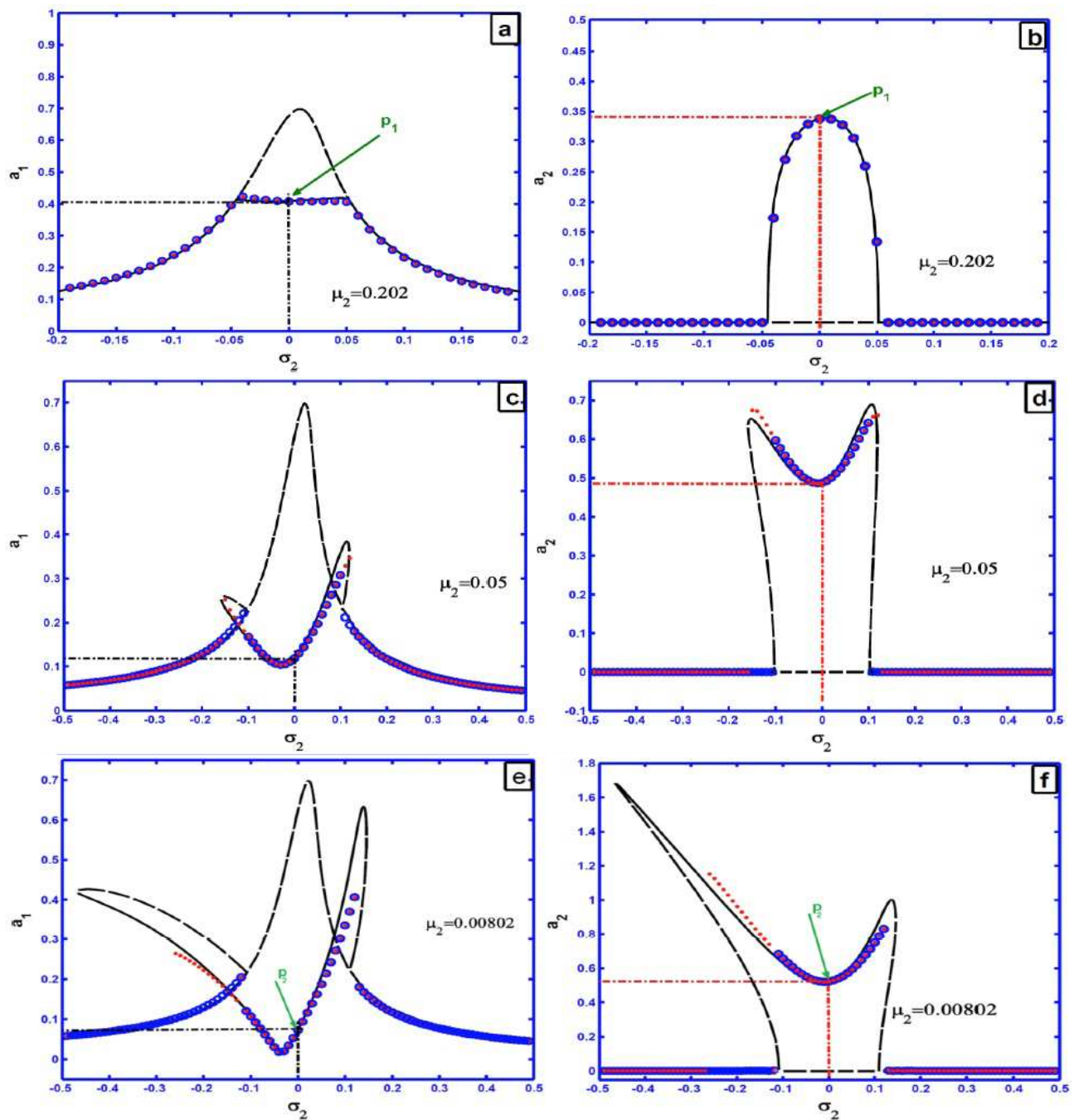


Fig. 12: Effect of decreasing the absorber linear damping coefficient μ_2 on the frequency-response curves: Duffing oscillator (left column), and pendulum (right column).

of an autoparametric pendulum-like mechanism subjected to harmonic excitation. They proposed a suspension composed of a semi-active MR damper and a nonlinear spring. Kecik [12] studied the nonlinear oscillations of autoparametric system consists of a nonlinear oscillator attached to a pendulum. A combination of MR damper

and a nonlinear spring made from a shape memory alloy are proposed.

In this paper, the system amplitude-phase modulating equations are extracted utilizing the multiple scales perturbation method. Bifurcation behavior of the system is explained in details. The effects of the coupling parameters, pendulum linear damping coefficient, and

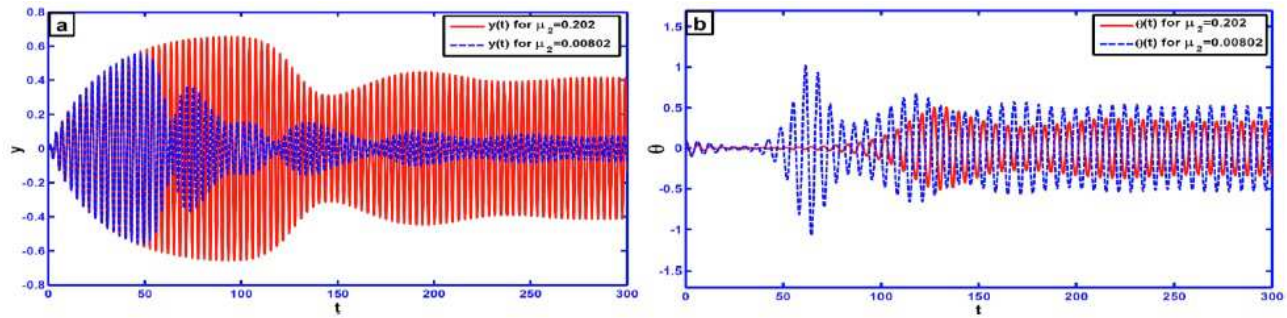


Fig. 13: System time-histories according to points P_1 and P_2 that showed on Fig. 12 and initial conditions $y(0) = \dot{y}(0) = \dot{\theta}(0) = 0$, $\theta(0) = 0.1$ of: (a) Duffing oscillator, and (b) pendulum.

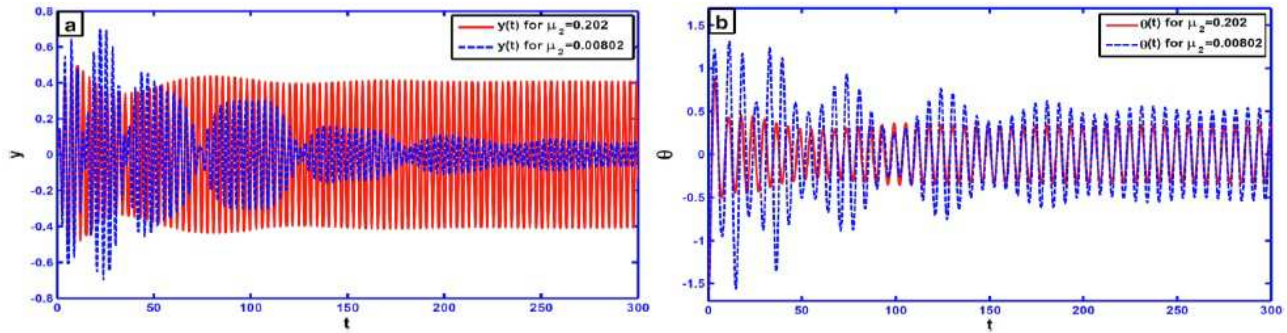


Fig. 14: System time-histories according to points P_1 and P_2 that marked on Fig. 12 at the initial conditions $y(0) = \dot{y}(0) = \dot{\theta}(0) = 0$, $\theta(0) = -\frac{\pi}{2}$: (a) Duffing oscillator, and (b) pendulum.

excitation amplitude on the system response curves are explored. Numerical confirmations for the all acquired results are performed. The time histories are conducted to show the exchange of energy between the two subsystems (i.e. Duffing oscillator and the pendulum). The optimal working conditions of such system are concluded. The force-response curve before and after attaching the pendulum to the oscillator is investigated for the first time, where an interesting phenomenon that is not reported before that is “At small negative detuning parameter (i.e. $-0.2 \leq \sigma_2 < 0$), beyond specific value of the excitation force (γ), the vibration amplitude of Duffing oscillator decreases as the excitation force increases”.

Acknowledgement

This research received no specific grant from any funding agency in the public, commercial, or not-for-profit sectors.

Compliance with Ethical Standards

Conflict of Interest The author declared no potential conflicts of interest with respect to the research, authorship, and/or publication of this article.

References

- [1] A. Nayfeh, D. Mook, L. Marshall, *Journal of Hydraulics* **7**, 145-152 (1973).
- [2] A. Haddow, A. Barr, D. Mook, *Journal of Sound and vibration* **97**, 451-473 (1984).
- [3] A. Nayfeh and L. Zavodeny, *Journal of Applied Mechanics* **110**, 706-710 (1988).
- [4] B. Balachandran and A. Nayfeh, *Nonlinear Dynamics* **2**, 77-117 (1991).
- [5] N. A. Saeed, W. A. El-Ganaini, M. Eissa, *Applied Mathematical Modelling* **37**, 8846-8864 (2013).
- [6] M. Eissa, N. A. Saeed, W. A. El-Ganaini, *Nonlinear Dynamics* **76**, 743-764 (2014).
- [7] J. Warminski and K. Kecik, *Mathematical Problems in Engineering* **Article ID 80705**, (2005).
- [8] J. Warminski and K. Kecik, *Journal of Sound and vibration* **322**, 612-628 (2009).
- [9] K. Kecik and J. Warminski, *Procedia IUTAM* **5**, 249-258 (2012).

- [10] K. Kecik and J. Warminski, Mathematical Problems in Engineering **Article ID 451047**, (2011).
- [11] K. Kecik, A. Mitura, D. Sado, J. Warminski, *Meccanica* **49**, 1887-1900 (2014).
- [12] k. Kecik, *International Journal of Non-Linear Mechanics* **70**, 63-72 (2015).
- [13] P. Brzeski, P. Perlikowski, S. Yanchuk, T. Kapitaniak, *Journal of Sound and Vibration* **331**, 5347-5357 (2012).
- [14] A. M. Gus'kov, G. Ya. Panovko, Chan Van Bin, *Journal of Machinery Manufacture and Reliability* **37**, 321-329 (2008).
- [15] Y. Song, H. Sato, Y. Iwata, T. Komatsuzaki, *Journal of Sound and Vibration* **259**, 747-759 (2003).
- [16] B. Banerjee, A. K. Bajaj, P. Davies, *International Journal of Non-Linear Mechanics* **31**, 21-39 (1996).
- [17] A. K. Bajaj, S. I. Chang, J. M. Johnson, *Nonlinear Dynamics* **5**, 433-457 (1994).
- [18] A. Vyas and A. K. Bajaj, *Journal of Sound and Vibration* **246**, 115-135 (2001).
- [19] H. Sheheitli and R. H. Rand, *Nonlinear Dynamics* **70**, 25-41 (2012).
- [20] P. Brzeski, P. Perlikowski, T. Kapitaniak, *Communications in Nonlinear Science and Numerical Simulation* **19**, 298-310 (2014).
- [21] T. Ikeda, *J. Comput. Nonlinear Dynam.* **6**, 1-11 (2011).
- [22] A. M. Tusset, F. C. Janzen, V. Piccirillo, R. T. Rocha, J. M. Balthazar, G. Litak, *Journal of Vibration and Control* (2017), <https://doi.org/10.1177/1077546317714882>.
- [23] A. Nayfeh and D. Mook, *Nonlinear Oscillations*, Wiley, New York, 1995.



Wedad Ali El-Ganaini is an Associate Professor of Mathematics at Department of Physics and Engineering Mathematics, Faculty of Electronic Engineering, Menoufia University, Egypt. She received her M. Sc. and Ph.D. degrees in numerical analysis, from Suez canal

University, Egypt. Her main research interests include numerical analysis, differential equations, mathematical modelling and their applications in engineering. She has published 35 research articles in reputed international journals of mathematical and engineering sciences. Dr. Wedad directed and advised many Ph.D. and M.Sc. postgraduate students.